Electronic Supplementary Information

A new perspective of the lanthanide metal–organic frameworks: tailoring Dy-BTC nanospheres for rechargeable Li-O_2 batteries†

Dan Liu,[a‡] Xinmin Zhang,[b‡] Yan-Jie Wang,[a*] Shuyan Song,[c] Lifeng Cui,[a] Hongbo Fan,[a] Xiaochang Qiao[a] and Baizeng Fang[d*]

[a]*School of Materials Science and Engineering, Dongguan University of Technology, No. 1, Daxue Rd, Songshan Lake, Dongguan, Guangdong, P. R. China. Email: wyj@dgut.edu.cn*

[b]*HEC R&D Center, Institute of Electronic Materials, Dongguan, Guangdong, P. R. China*

[c]*State Key Laboratory of Rare Earth Resource Utilization, Changchun Institute of Applied Chemistry, Chinese Academy of Sciences, Changchun, Jilin, China.*

[d]*Department of Chemical & Biological Engineering & Clean Energy Research Center, University of British Columbia, 2360 East Mall, Vancouver, B.C. V6T 1Z3, Canada. Email: bfang@chbe.ubc.ca*

† Electronic supplementary information (ESI) available. See DOI: 10.1039/x0xx00000x

‡ These authors have contributed equally to this work.

Table S1. Distortion values calculated for the Dy^{III} ions geometry.

	Hexacoordinate	S(C_{5v})	S(O_h)	S(D_{3h})
Dy-BTC	Dy1	15.22	10.04	5.64

S = symmetry

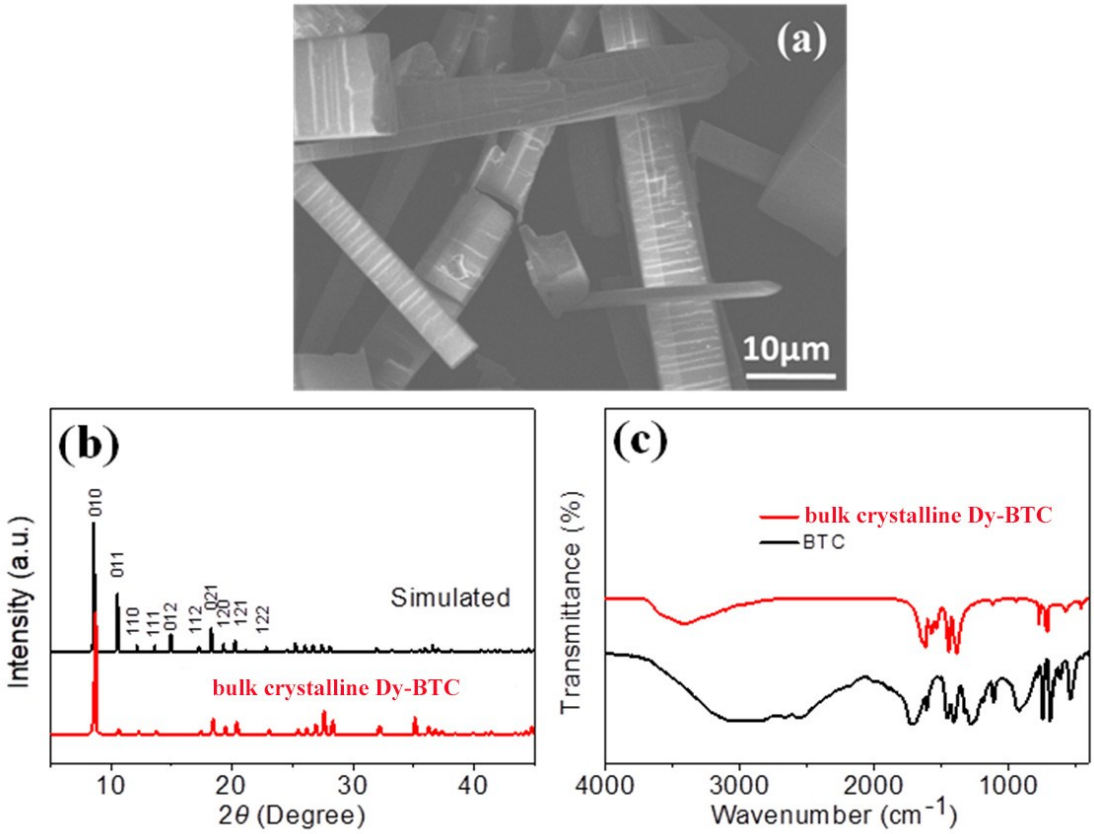

Figure S1. a) The SEM image of the bulk crystalline Dy-BTC, b) PXRD patterns and c) FTIR spectra.

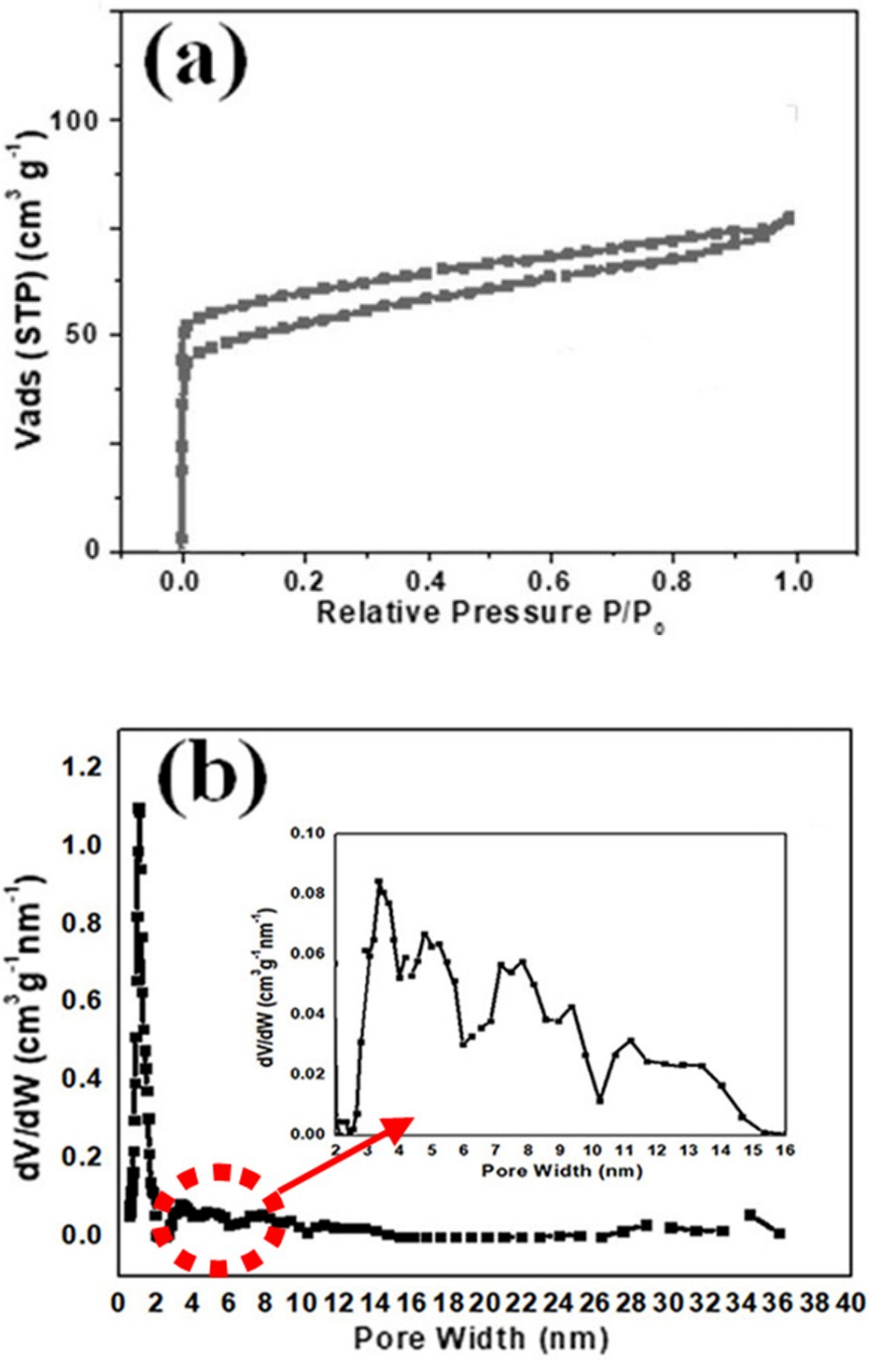

Figure S2. a) Low-pressure N_2-adsorption isotherms at 77 K and b) the pore size distribution for the bulk crystalline Dy-BTC (the insert shows the enlarged plot of the marked area with red circle).

Evidently, the bulk crystalline Dy-BTC is dominated by micropores although a small fraction of mesopores exist.

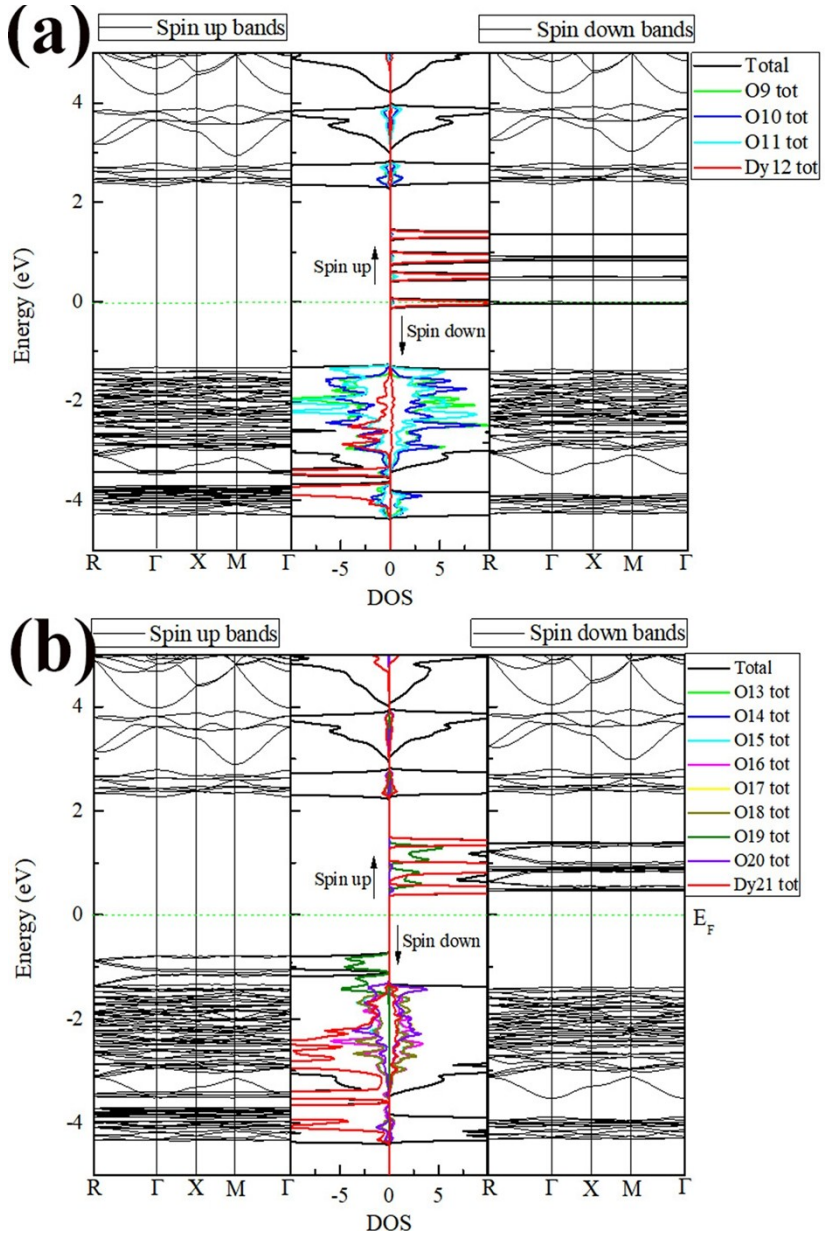

Figure S3. Band structure and DOS of a) Dy-BTC and b) Dy-BTC-O (i.e., Dy-BTC after O_2 adsorption).

To reveal the microscopic mechanism of the excellent performance of Dy-BTC, we performed the first-principles calculations of oxygen adsorption energy and electronic structure of Dy-BTC as well as its after adsorption of O_2. We noticed that it exists unoccupied *f* orbitals around Fermi level in the electronic structure of Dy-BTC (Figure S3a). It is considered that these unoccupied *f* orbitals are prone to coordinate with O_2. Comparing the electronic structures between Dy-BTC and its after O_2-adsorption (Figure S3b), we discover, yet again that the unoccupied orbitals around Fermi level shift under the Fermi level due to its coordination with O_2. Thus, we could conclude that the unoccupied *f* orbitals play an important role in the process of adsorption of O_2.

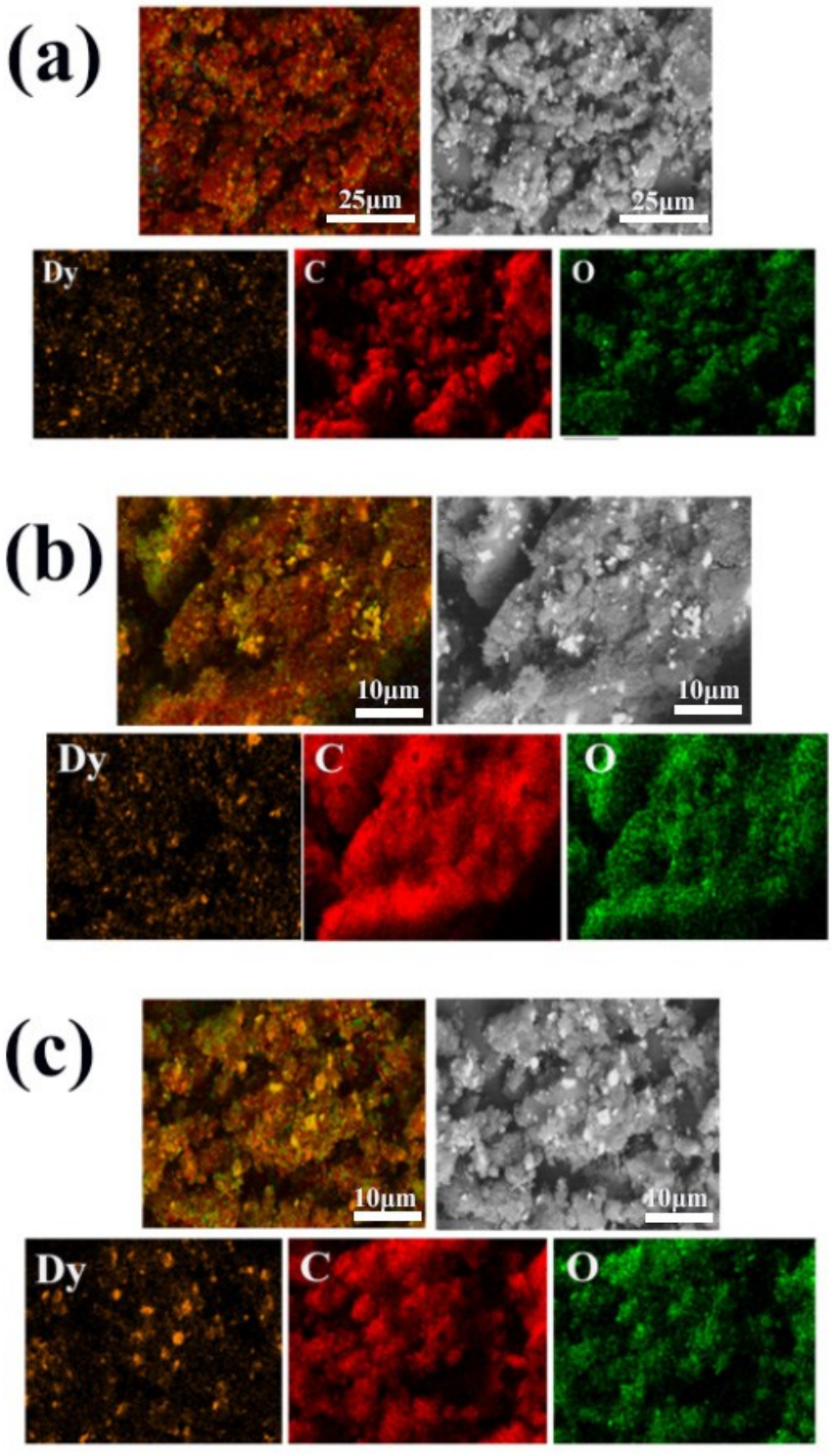

Figure S4. SEM images and EDX mappings of the Dy-BTC nanospheres-super P composite electrode at different stages: a) before discharge; b) after discharge; c) after charge.

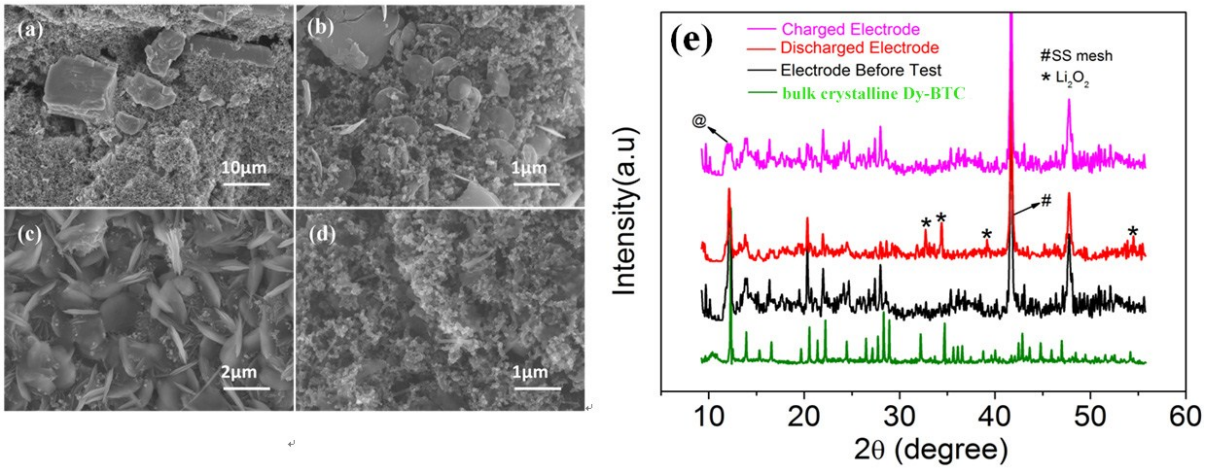

Figure S5. SEM images of the bulk crystalline Dy-BTC-super P composite electrode: a) before the test; b) half discharged; c) fully discharged; (d) fully charged; e) XRD patterns of the electrode at different test states. The diffraction peaks located at 12.5° (the characteristic peak of Dy-BTC MOFs marked by @) disappeared after fully charging implying that the bulk crystalline Dy-BTC collapsed after being recharged, which is consistent with the observation from the SEM image shown in Figure S4d.

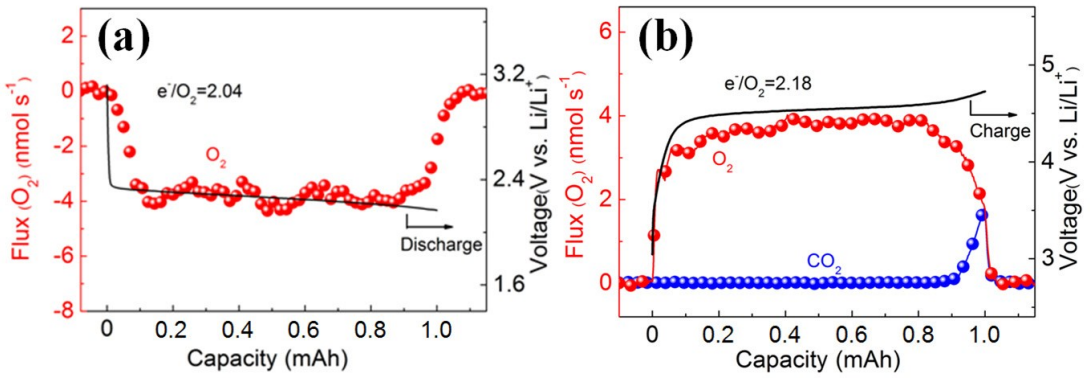

Figure S6. DEMS of the bulk crystalline Dy-BTC-based electrode during a) discharge and b) charge.

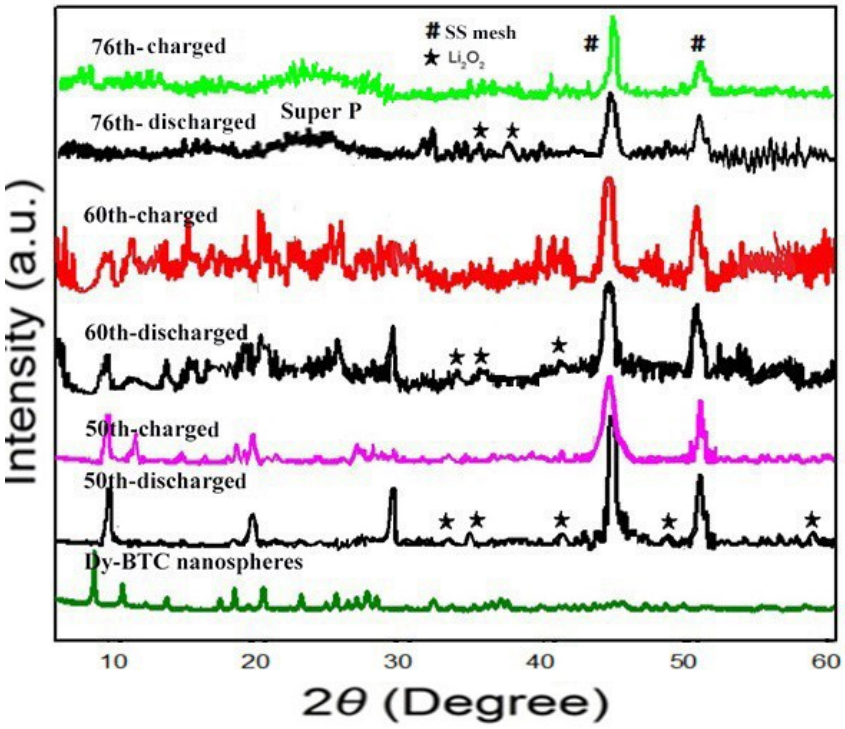

Figure S7. XRD patterns of the Dy-BTC nanospheres-super P composite electrode after the 50th, 60th and 76th cycle of charge/discharge.

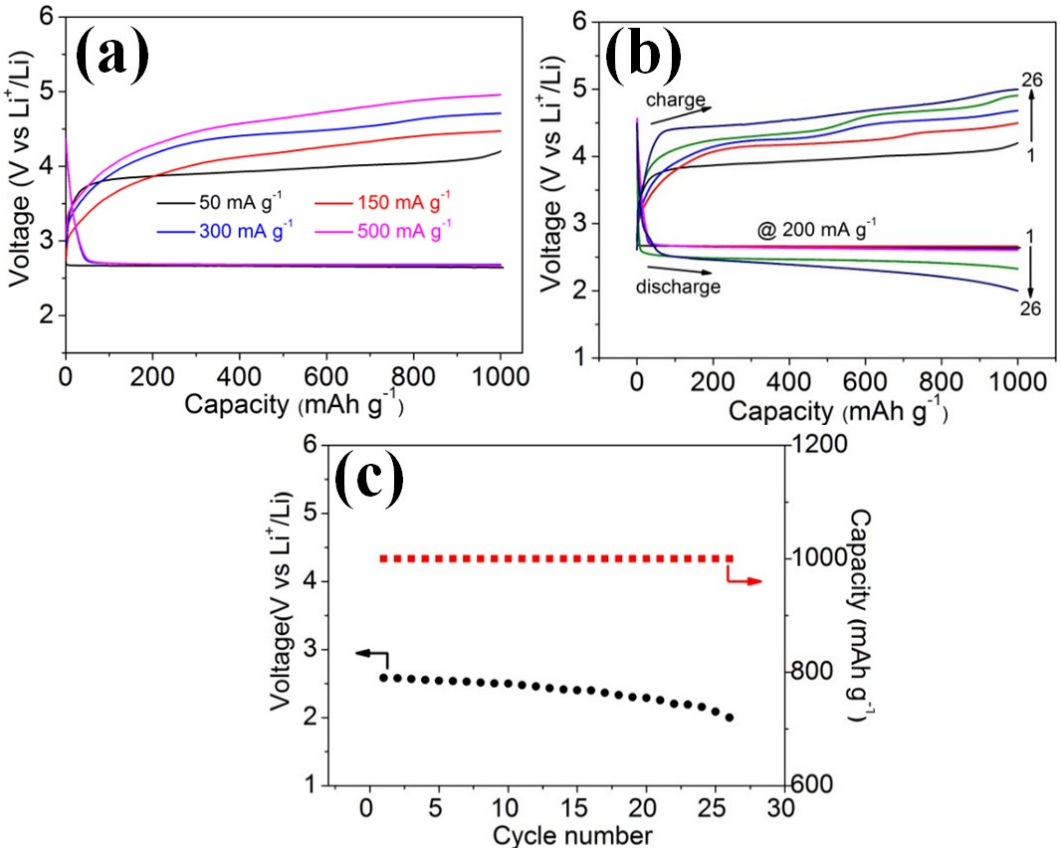

Figure S8. a) Rate capability of the bulk crystalline Dy-BTC-based electrode in pure O_2 with a fixed capacity of 1000 mAh g^{-1}; b) Representative cycling response of the bulk crystalline Dy-BTC-based electrode under the specific capacity limit of 1000 mAh g^{-1}, with discharge/charge curves at cycle 1, 5, 10, 25, and 26 shown. Current: 200 mA g^{-1}; c) Discharge voltage and capacity retention *vs*. cycle number.